Release of immunomodulatory peptides at bacterial membrane interfaces as a novel strategy to fight microorganisms

Thiago Viana de Freitas[1], Utsa Karmakar[2], Andreanne G. Vasconcelos[3], Michele A. Santos[1,4], Bianca Oliveira do Vale Lira[5,6], Samuel Ribeiro Costa[1], Eder Alves Barbosa[1], José Cardozo-Fh[7], Rafael Correa[8], Dalila J. S. Ribeiro[8], Maura Vianna Prates[7], Kelly G. Magalhães[8], Marcelo Henrique Soller Ramada[5,6], José Roberto de Souza Almeida Leite[3], Carlos Bloch Jr[7], Aline Lima de Oliveira[4], Marc Vendrell[2], and Guilherme Dotto Brand[1,*]

From the [1]Universidade de Brasília, Instituto de Química, Laboratório de Síntese e Análise de Biomoléculas, LSAB, Brasília, Distrito Federal, Brasil; [2]Centre for Inflammation Research, The University of Edinburgh, Edinburgh, UK; [3]Universidade de Brasília, Faculdade de Medicina, Núcleo de Pesquisa em Morfologia e Imunologia Aplicada, NuPMIA, Brasília, Distrito Federal, Brasil; [4]Universidade de Brasília, Instituto de Química, Laboratório de Ressonância Magnética Nuclear, LRMN, Brasília, Distrito Federal, Brasília, Brasil; [5]Programa de Pós-Graduação em Ciências Genômicas e Biotecnologia, and [6]Programa de Pós-Graduação em Gerontologia, Universidade Católica de Brasília, Brasília, Distrito Federal, Brasil; [7]Laboratório de Espectrometria de Massa, LEM, Embrapa Recursos Genéticos e Biotecnologia, Brasília, Distrito Federal, Brasil; [8]Universidade de Brasília, Instituto de Biologia, Laboratório de Imunologia e Inflamação, LIMI, Brasília, Distrito Federal, Brasil

Cationic and amphiphilic peptides can be used as homing devices to accumulate conjugated antibiotics to bacteria-enriched sites and promote efficient microbial killing. However, just as important as tackling bacterial infections, is the modulation of the immune response in this complex microenvironment. In the present report, we designed a peptide chimaera called Chim2, formed by a membrane-active module, an enzyme hydrolysis site and a formyl peptide receptor 2 (FPR2) agonist. This molecule was designed to adsorb onto bacterial membranes, promote their lysis, and upon hydrolysis by local enzymes, release the FPR2 agonist sequence for activation and recruitment of immune cells. We synthesized the isolated peptide modules of Chim2 and characterized their biological activities independently and as a single polypeptide chain. We conducted antimicrobial assays, along with other tests aiming at the analyses of the cellular and immunological responses. In addition, assays using vesicles as models of eukaryotic and prokaryotic membranes were conducted and solution structures of Chim2 were generated by ^{1}H NMR. Chim2 is antimicrobial, adsorbs preferentially to negatively charged vesicles while adopting an α-helix structure and exposes its disorganized tail to the solvent, which facilitates hydrolysis by tryptase-like enzymes, allowing the release of the FPR2 agonist fragment. This fragment was shown to induce accumulation of the cellular activation marker, lipid bodies, in mouse macrophages and the release of immunomodulatory interleukins. In conclusion, these data demonstrate that peptides with antimicrobial and immunomodulatory activities can be considered for further development as drugs.

Membrane-active peptides (MAPs) are versatile tools (1, 2). While they are usually considered for their capacity to penetrate cells and/or their antimicrobial activity (3), some MAPs can also induce or hinder (4) membrane fusion processes while others can nucleate the formation of membrane-associated amyloid aggregates (5). These features grant MAPs a range of putative biotechnological applications, which can be further expanded by their combination with other classes of molecules (6), such as organometallics (7), radioactive labels (8), and conventional antibiotics (9, 10).

One interesting feature of MAPs is that, given their usual cationic and amphiphilic nature (1, 11, 12), some molecules can accumulate preferentially in microorganism membranes when compared to eukaryotic cells (9, 13, 14). Therefore, besides acting as direct antimicrobials, they can be used to increase the effective concentration of pharmaceuticals in microenvironments with accumulation of pathogenic bacteria (9, 10). This represents an alternative to their use as membranolytic agents, which requires micromolar concentrations at the infection site even at relatively low bacterial cell counts (15). The basis of such discrimination is the differential membrane composition of prokaryotes and eukaryotes. Negatively charged lipopolysaccharides (LPS), teichoic acids, and phospholipids provide an overall negative net charge to the surface of bacteria, which can, mostly by electrostatic forces, screen positively charged ions and molecules. In contrast, eukaryotic cell membranes are composed mostly of zwitterionic phospholipids, neutral at physiological pH, which typically results in lower affinity to positively charged molecules (11). Indeed, some MAPs have been considered homing devices for the detection of *in vivo* bacterial infections. This is the case of the peptide UBI29–41 (TGRAKRRMQYNRR),

* For correspondence: Guilherme Dotto Brand, gdbrand@unb.br.

obtained from the ubiquicidin protein, which was radiolabeled and used for the *in vivo* tracing of *Staphylococcus aureus*-infected sites (16). Also, the same peptide esterified to chloramphenicol, was shown to be more effective than the drug alone in the resolution of infection caused by *S. aureus* in mice (9). This was attributed to a more efficient accumulation of the antibiotic at the infection sites.

Another relevant aspect when designing bacteria-targeting MAPs or other peptide-drug conjugates is their susceptibility to enzymatic hydrolysis in the biological medium (17). Although considered exclusively a drawback, peptide hydrolysis can also be strategically explored to design targeted prodrugs (18). Bacteria-infected tissues are under intense proteolysis by enzymes secreted by both bacteria and the host. This was explored by a construct where the peptide UBI29-41 is linked to the antibiotic colistin through a neutrophil elastase susceptible linker, aiming thus the release of free colistin at infected tissues (10). In vertebrates, not only neutrophil elastase but also many other enzymes involved in the inflammatory and complement cascades become highly abundant at bacterial infection sites. Some of these enzymes present trypstase-like activity (19), like KLK enzymes and C3 convertase (20–22). These enzymes can be used for the local release of peptide-linked antimicrobial drugs or for the release of peptide fragments that stimulate the immune system by inducing chemotaxis and the maturation of host immune cells. One attractive target for the activation of the host immune system is the formyl peptide receptor 2 (FPR2) (23, 24). This receptor belongs to the G-protein coupled receptor family and their activation is relevant to leukocyte influx in early infection

events by *S. aureus* (25). In addition, FPR2 activation has been shown to promote higher survival in mice submitted to sepsis by cecal ligation and puncture (26). FPR2s are promiscuous and can be activated by many endogenous and exogenous ligands, such as the lipoxin A4 (LPXA4), the amyloid serum protein A, the cathelicidin LL-37, or even synthetic peptides from the W series (23). Interestingly, the downstream signaling can be either proinflammatory or anti-inflammatory, depending on the agonist (27). The W peptide series, mostly WKYMVm, are well-known agonists and have been shown to promote the chemotaxis of resting immune cells (28). Also, some simple W peptide analogs, containing exclusively L-amino acids, have been described in the literature. One of them was the peptide WKYM-NH$_2$, which was capable of selectively activating FPR2 at nanomolar concentrations (29).

In the present report, we introduce a chimaeric peptide molecule, named Chim2, which combines three bioactive modules in a single polypeptide chain (Fig. 1). The Chim2a module is membrane-active and aims at the preferential accumulation in prokaryotic membranes. This module is based on the intragenic antimicrobial peptide (30–32) Hs02, a cationic and amphiphilic segment from the human unconventional myosin 1 h protein with broad and potent antimicrobial activity (31). Chim2b is a spacer module containing a -GG- dyad, for increased backbone flexibility, and an enzymatic hydrolysis site for tryptase-like enzymes, -KR-. This was based on the broad occurrence of bacterial-secreted enzymes with tryptase-like activity (*e.g.*, Omptin) (33) and the presence of human kallikrein (KLK) enzymes with such specificity in inflamed tissues (20). At last, Chim2c is a FPR2 peptide agonist, designed to
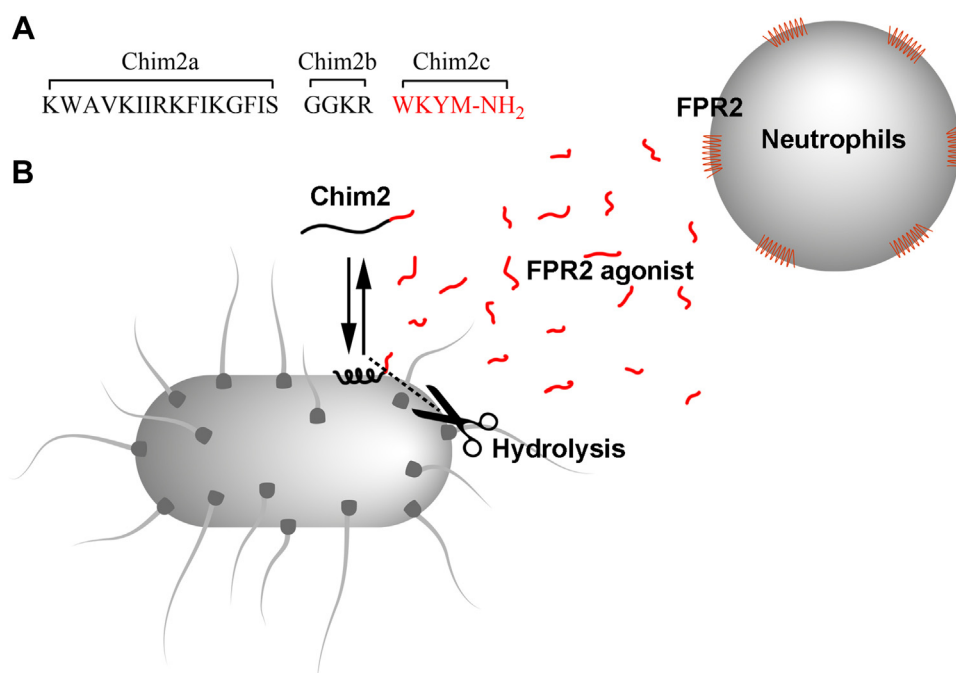
Figure 1. Mode of action of the peptide Chim2. *A*, Chim2 (KWAVKIIRKFIKGFISGGKRWKYM-NH$_2$) was rationally designed as a chimaera formed by three modules: An N-terminal membrane-active module, called Chim2a (KWAVKIIRKFIKGFIS), a spacer module also containing a trypsin hydrolysis domain (-GGKR-), called Chim2b and a C-terminal module (WKYM-NH$_2$, in *red*) consisting of a FPR2 agonist peptide (Chim2c). *B*, Chim2 was designed to accumulate preferentially on the surface of bacterial cells and go through a coil-helix transition, mostly at the Chim2a domain. This should expose the unstructured trypsin hydrolysis site in Chim2b, which, after hydrolysis, releases Chim2c, an FPR2 agonist WKYM-NH$_2$ (in *red*). The Chim2c FPR2 agonist peptide should diffuse from the bacterial focal point and activate FPR2 in neutrophils (7TM receptors in *red* in cells). FPR, formyl peptide receptor.

activate FPR2 receptors in immune cells at the infection site after Chim2 hydrolysis, producing or reinforcing a chemotactic gradient for leukocyte migration. For that, the peptide WKYM-NH$_2$ was chosen due to its reported nanomolar affinity and selectivity toward FPR2 (29). We investigated the biological activity of Chim2, first by studying its isolated modules and then the chimaeric peptide itself. For such, the peptide Chim2 was chemically synthesized, and its structure was evaluated in buffer and after adsorption to neutral (1,2-dimyristoyl-sn-glycero-3-phosphocholine [DMPC]), and negatively charged (2:1 1,2-dimyristoyl-sn-glycero-3-phospho-(1'-rac-glycerol) [DMPC:DMPG]) phospholipid vesicles used as models of eukaryotic and prokaryotic cells, respectively. Furthermore, ^{1}H NMR solution structures of Chim2 bound to dodecylphosphocholine (DPC) micelles were generated. Differential Chim2 trypsinolysis assays in media containing neutral and negatively charged vesicles were conducted, with the concomitant characterization of Chim2-hydrolyzed fragments by LC and MALDI-TOF/MS. Last, the capacity of Chim2 and some of its fragments to induce the formation of radical oxygen species (ROS) in human neutrophils was assayed. Our data indicate that Chim2 is antimicrobial, adsorbs preferentially in negatively charged vesicles and, upon interaction, exposes the disorganized Chim2b domain, which, once cleaved by trypsin, releases Chim2c. Altogether, these data demonstrate that the strategy presented herein is sound and that peptides from the Chim series are actual candidates for further development as peptide drugs combined antimicrobial and immunomodulatory activity.

Results

The Chim2a module is membrane-active

The membrane-active module of Chim2 is based on the peptide Hs02, primary structure KWAVRIIRKFIKGFIS-NH$_2$. This peptide was previously shown to assume an α-helical structure upon model membrane interaction, presenting also broad and potent antimicrobial and LPS-suppressing activities (31). To further investigate the adequacy of Hs02 as the membrane-active module of Chim2, we titrated it with DMPC and 2:1 DMPC:DMPG large unilamellar vesicles (LUVs) and recorded the far-UV CD spectra of the samples in a spectropolarimeter. Hs02 was unstructured in phosphate buffer but transitioned to an α-helical conformation upon model membrane addition, with the characteristic positive peak at around 190 nm and the negative minima in 208 and 222 nm (Fig. 2, *A* and *B*). However, whereas the addition of 2:1 DMPC:DMPG LUVs at 320 μM concentration (8:1 lipid:peptide ratio) resulted in nearly 40% of the maximum theoretical α-helical structure for Hs02, vesicles made solely of DMPC in the same concentration resulted in only 22% α-helical structure (Fig. 2C). Higher Hs02 percent structuration following titration with DMPG-enriched vesicles was also observed at 4:1 and 2:1 lipid:peptide ratios. Nevertheless, after the addition of 2000 μM of either DMPC or 2:1 DMPC:DMPG LUVs (50:1 lipid:peptide ratio), Hs02 was nearly 45% α-helical for both membrane compositions, indicating that, for this peptide, selectivity toward negatively charged membranes might be lost at higher lipid:peptide ratios.
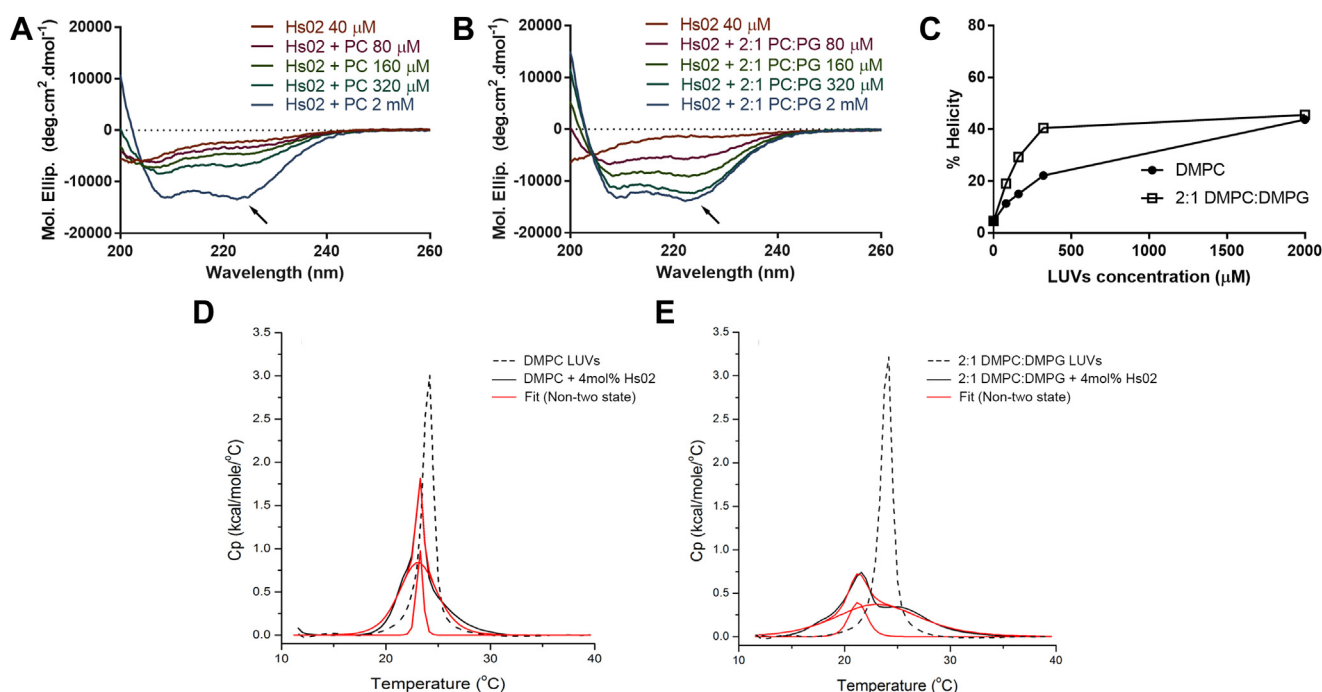
Figure 2. Hs02 interacts differentially with large unilamellar vesicles made of DMPC and 2:1 DMPC:DMPG (w/w). Far-UV CD spectra of Hs02 at 40 μM concentration in buffer and titrated with increasing concentrations of (*A*) DMPC LUVs and (*B*) 2:1 DMPC:DMPG. Continuous lines in *red* represent the result obtained for buffer; in *purple*, 80 μM LUVs, in *olive*, 160 μM LUVs, in *green*, 320 μM LUVs, and in *blue*, 2000 μM LUVs. *C*, percent helicity of Hs02 as a function of lipid concentration. Heating thermal scans of (*D*) DMPC LUVs and (*E*) 2:1 DMPC:DMPG LUVs enriched with 4 mol% Hs02. *Black discontinuous lines* correspond to the heating thermal scans of corresponding LUVs without any added peptide. *Black continuous lines* correspond to experimental data for LUVs enriched with Hs02. *Red lines* correspond to a non-two-state model fitting with two components of the main phase transition of model vesicles (numerical results can be found as supporting information, Table S1). LUV, large unilamellar vesicle.

Design of a membrane-active immunomodulatory peptide

Thermal heating scans were obtained for LUVs enriched with Hs02 at 0.04 mol/mol (25:1 lipid:peptide ratio). The heating thermal scan of DMPC LUVs resulted in an endotherm compatible with the $P'_\beta \rightarrow L_\alpha$ main phase transition and this was fit to a non-two-state model with two peaks (Fig. 2D, black discontinuous line), as previously reported by our group and others (30, 34, 35). Adding Hs02 to DMPC LUVs altered the main phase transition of vesicles, reducing the transition temperature of the sharp component (Tm1) and producing an overall broadening of the second component (Fig. 2D, black lines, model fitting in red). These changes are compatible with the peptide interaction with the interfacial portion of the membrane. The same experiments were performed with 2:1 DMPC:DMPG LUVs (Fig. 2E). Hs02 altered the main phase transition of LUVs (black, discontinuous line) further reducing the Tm of the sharp component and producing a more pronounced broadening of the phase transition in relation to the zwitterionic DMPC LUVs (Fig. 2, D and E, black lines). The thermal profile suggests a deeper peptide interaction with the membrane in DMPG-enriched LUVs. However, since the overall transition enthalpy (ΔH_{cal}) remained largely unaltered (Table S1), this peptide presented no significant detergency effect, reinforcing that this peptide interacts more pronouncedly with the interfacial region of membranes of both assayed compositions.

Overall, these results suggest that Hs02 possesses a concentration-dependent discriminatory capability toward membranes containing the negatively-charged phospholipid DMPG. Furthermore, they confirm previous observations that Hs02 interacts superficially with membranes (31) and can be used as a preliminary membrane-targeting module for the rational design of chimaeric molecules.

## The Chim2c module stimulates mice bone marrow derived macrophages

The peptide WKYM-NH$_2$, Chim2c in the current work, was reported as the core sequence for W peptides in the activation of human FPR2 (29), being capable of selective activation of FPR2 over FPR1. This peptide was synthesized, purified (Figs. S4–S6), and tested as an elicitor in mouse bone marrow derived macrophages (BMDM). BMDMs were incubated or not with peptide WKYM-NH$_2$ at 10 μM concentration and the cellular activation markers, lipid bodies, were quantified by flow cytometry. As a control, cells were incubated with LPS and lipid bodies were also quantified. Both treatments, WKYM-NH$_2$ and LPS, triggered cell activation by inducing lipid bodies biogenesis in BMDMs (Fig. 3A). The interleukins-12 (IL-12) and interleukins-6 (IL-6) were quantified after the stimulation of BMDMs with both the peptide Hs02, the basis of the Chim2a module, and Chim2c, at 10 μM concentration (Fig. 3, B and C). Again, LPS was used as a positive control. While the incubation of BMDMs with Hs02 elicited the release of a small, but significant amount of IL-12, the same was not observed for IL-6. In contrast, cells incubated with WKYM-NH$_2$ released IL-6 and IL-12 in similar levels to those incubated with LPS, indicating that the Chim2c module is indeed capable of stimulating proinflammatory response in mouse BMDM in the assayed conditions.

The peptide Chim2

Peptide Chim2, primary structure KWAVKIIRKFIKGFI SGGKRWKYM-NH$_2$, was chemically synthesized by solid-phase peptide synthesis, purified by preparative chromatography, and analyzed by MS, as demonstrated in the supporting information, Figs. S1–S3. Its primary structure consists in Chim2a or the intragenic antimicrobial peptide Hs02 with a conservative Arg5Lys substitution; Chim2b, the spacer plus trypsin-hydrolysis site (-GGKR-); and Chim2c, the core FPR2 agonist peptide WKYM-NH$_2$, all in a single polypeptide chain.

Paramount to the application of Chim2 as a selective peptide is its capacity to bind differentially to negatively charged membranes in relation to their neutral counterparts. To investigate that, Chim2 was titrated with increasing concentrations of DMPC and 2:1 DMPC:DMPG LUVs, as models of eukaryotic and prokaryotic cells, respectively. Far-UV CD spectra were acquired for the peptide alone and after titrations with LUVs (Fig. 4, A and B). Chim2 presented a random coil
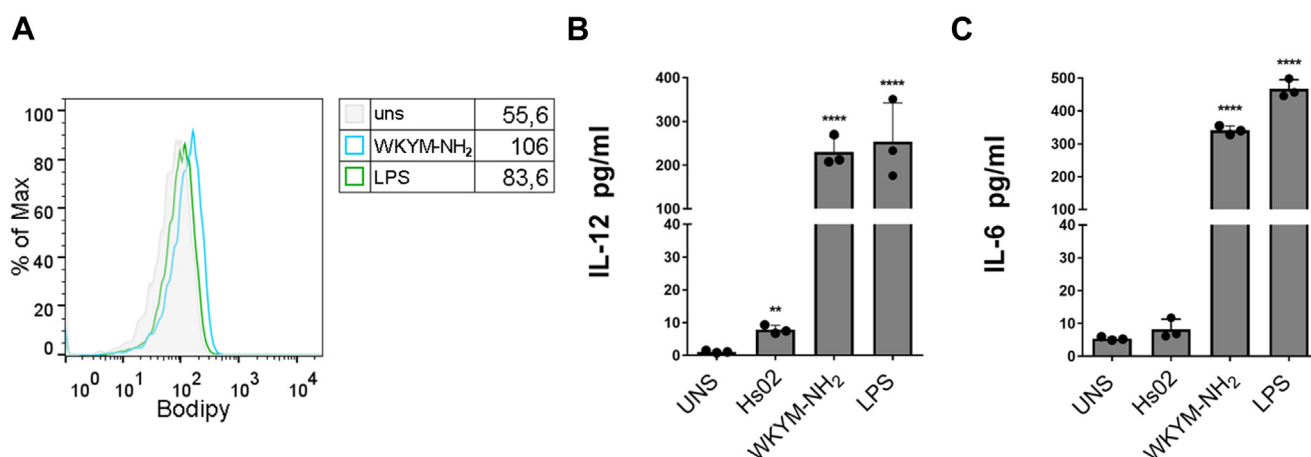
Figure 3. Peptide WKYM-NH$_2$ (Chim2c) induces the synthesis of lipid bodies and the release of interleukins in mouse BMDMs. *A*, lipid bodies were quantified in unstimulated BMDM, as well as cells challenged with LPS (500 ng/ml, 24 h) and with the peptide WKYM-NH$_2$ (10 μM). In addition, ELISA assays were made to quantify IL-12 (*B*) and IL-6 (*C*) in unstimulated cells and in BMDM stimulated with LPS 1 μg/ml, 10 μM Hs02, and 10 μM WKYM-NH$_2$. Values were expressed as means ± SEM. **$p < 0.01$; ****$p < 0.0001$ *versus* unstimulated (UNS) control group.

pattern in buffer, being therefore unstructured. Titrating Chim2 with DMPC vesicles, up to 2 mM concentration, introduced changes in the far-UV CD spectra that are typical of α-helical structure (Fig. 4A). Nevertheless, little structuration was observed after DMPC titration, and Chim2 was only 13% α-helical at 2 mM DMPC LUVs. In contrast, adding negatively charged 2:1 DMPC:DMPG LUVs to a Chim2 solution induced a more marked effect, especially at higher phospholipid concentrations (Fig. 4B). Indeed, Chim2 was 55% α-helical in 2 mM 2:1 DMPC:DMPG LUVs, indicating that the peptide structuration as an α-helix is facilitated by the presence of the negatively-charged phospholipid DMPG. Altogether, these results indicate that Chim2 is more selective toward DMPG-containing membranes than Hs02, probably due to the Arg5Lys mutation and the insertion of the disordered Chim2b and Chim2c domains.

A more detailed structure of Chim2 following its interaction with DPC-d38 micelles was obtained by solution ^{1}H NMR spectroscopy (Fig. 4, C–F). Despite its zwitterionic composition, DPC micelles have higher curvature than DMPC LUVs, a feature that facilitates peptide adsorption and consequently induces higher α-helical structuration, as previously observed by our group and others (31, 32). TOCSY and NOESY spectra allowed the identification and assignment of the spin systems of 21 out of 24 amino acid residues (Figs. S13 and S14; Tables S2 and S3). The spin system of Lys[1], Gly[17] and Gly[18]
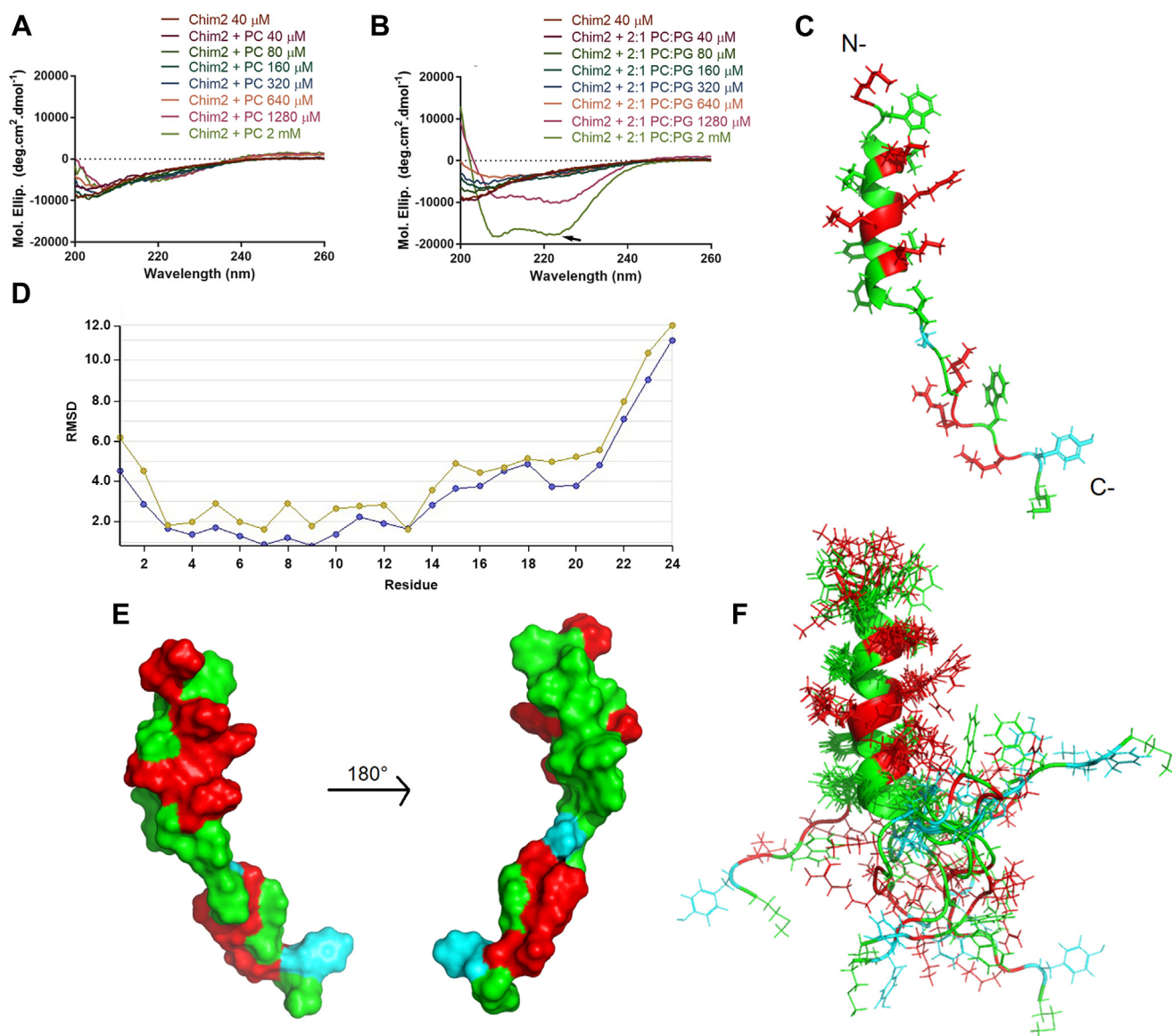
Figure 4. Structure of the peptide Chim2 in phospholipid vesicles and micelles. Far-UV CD spectra of 40 μM Chim2 added with (A) DMPC LUVs or (B) 2:1 DMPC:DMPG LUVs. *Continuous lines* in *red* represent the result obtained for buffer; in *purple*, 40 μM LUVs, in *dark green*, 80 μM LUVs, in *olive*, 160 μM LUVs, in *blue*, 320 μM LUVs, in *orange*, 640 μM, in *magenta*, 1280 μM, and in *green*, 2000 μM LUVs. C, ribbon representation of the lowest energy structure of Chim2 in the presence of DPC-d38 micelles. D, RMSD profile of the Chim2 peptide along its primary structure. E, surface hydrophobic feature of the Chim2 peptide. The structure on the right side shows the molecule rotated 180° around the vertical axis. F, backbone alignment of the final ten lowest-energy structures of Chim2. Side chain amino acid properties are shown in the following color code: *red* for the positively charged residues, *cyan* for the polar residues and *green* for the hydrophobic residues. (PDB: 8EB1). DPC, dodecylphosphocholine; LUV, large unilamellar vesicle.

amino acids could not be found, indicating that these belong to unstructured regions. The chemical shifts are reported in supporting information (Fig. S15) and the structures were deposited in Biological Magnetic Resonance Bank with access number 8EB1.

^{1}H NMR spectroscopy data show that Chim2 adopts an α-helical conformation from Ala^{3} to Phe^{14}, which is consistent with the structure displayed by Hs02 in the same environment (31). The ribbon representation of the structure of Chim2 is depicted in Figure 4C. Indeed, the structuration of the Chim2a module evidences its amphiphilic pattern (Fig. 4, C–F). Medium-range NOEs, specifically dαN(I, i + 3), dαN(i, i + 4) NOE, were present in the NOESY spectra of this part of the molecule, as commonly observed in other α-helical peptides. These results were also consistent with the secondary structure calculated by the chemical shift index of Hα backbone atoms (Fig. S15). However, Chim2 also presented an unstructured region, starting from Ile^{15} up to Met^{24}, which constitutes the Chim2b and Chim2c regions (-ISGGKRW-KYM-NH2). This is evidenced by the higher RMSD calculated for this part of polypeptide chain (Fig. 4D).

An ensemble of micelle-bound structures was calculated using 343 inter-proton distance restraints (Fig. 4F) and the statistical analyses of the best 10 NMR structures of Chim2 can be found as supporting information, Table S3. Statistical analyses, such as RMSD calculations, were made only for the α-helical domain of Chim2, since the C-terminal tail presents large structural flexibility. In the α-helical region of Chim2, Ramachandran plots show that the dihedral angles of 78% of all amino acid residues are in the most favored regions, while 18% are in allowed regions. The dihedral angles of amino acid residues in the unstructured regions were more scattered in the Ramachandran plot, and some residues, such as Gly^{17}, Gly^{18}, were frequently found in disallowed regions. This is consistent with their structural flexibility since the spin system for these residues could not be found in the spectra.

Binding to negatively charged LUVs directs trypsin hydrolysis of Chim2 to the Chim2b site

The peptide Chim2 was designed to bind preferentially to negatively charged membranes and, due to the steric hindrance imposed by the membrane interface on the Chim2a domain, direct the enzymatic activity to the trypsin hydrolysis site in Chim2b. Following trypsin hydrolysis in the spacer sequence, more specifically in -GGKR↓, the peptide Chim2c (WKYM-NH$_2$) should be released to the medium. To investigate this hypothesis, DMPC and 2:1 DMPC:DMPG LUVs at 1 mM concentrations were individually added to a 100 μM Chim2 solution (10:1 lipid:peptide ratio), followed by the addition of trypsin at 1 μg/ml. Control experiments without phospholipid vesicles were also performed. Samples were incubated at 37 °C, and aliquots were obtained in a time-resolved fashion, from 0 to 240 min. The Chim2 hydrolysis profile was qualitatively evaluated by MALDI-TOF/MS and quantitatively by HPLC (Fig. 5). The addition of trypsin to the

Chim2 solution in buffer, without any added vesicle, resulted in the complete hydrolysis of Chim2 in 60 min, with the subsequent release of 43.0 ± 9.4 μM WKYM-NH$_2$ at this time point (Fig. 5, A and B). MALDI-TOF/MS analysis evidences that various Chim2 trypsin fragments can be detected after 60 min of incubation, including [M + H]$^{+}$ = 626.322 Da, WKYM-NH$_2$, and [M + H]$^{+}$ = 821.481 Da, GFISGGKR (corresponding MS/MS spectra available as supporting information, Figs. S16–S18), as evidenced in Figure 5C. Indeed, in this reaction conditions, the concentration of WKYM-NH$_2$ peaked at 30 min (76.0 ± 10.0 μM) being this peptide further hydrolyzed by trypsin probably due to the internal hydrolysis site (WK↓YM-NH$_2$). The addition of 1 mM DMPC LUVs to the Chim2 solution prior to trypsin did not produce a marked alteration in the peptide hydrolysis kinetics when compared to Chim2 incubated with trypsin in buffer alone (Fig. 5A, red line). A fast Chim2 hydrolysis was observed and the release of the fragment WKYM-NH$_2$ followed a similar profile, as demonstrated in Figure 5D. Also, the Chim2 fragments detected by MALDI-TOF/MS were compatible with the control experiment (with no added vesicles), except for some additional ions from the phospholipid DMPC (Fig. 5E).

The addition of 1 mM 2:1 DMPC:DMPG LUVs altered significantly the kinetics of hydrolysis of Chim2. After 60 min of sample digestion, only 19.3 ± 2.5 μM WKYM-NH$_2$ was hydrolytically released to the medium, and contrary to the previously assayed conditions, Chim2 was still present, as evidenced by the HPLC profile and MALDI-TOF/MS data (Fig. 5, F and G). Indeed, even at the longest time-point assayed in this experiment (240 min), Chim2 was still detected. A second experiment was conducted using 25 μM Chim2 and 1 mM 2:1 DMPC:DMPG LUVs (40:1 lipid:peptide ratio) with longer incubation times (up to 480 min), followed by the quantification of both Chim2 and WKYM-NH$_2$ (Fig. 5H). This experiment was designed to verify the WKYM-NH$_2$ release kinetics at higher lipid:peptide ratios and therefore to better investigate whether Chim2 is being hydrolyzed by trypsin in solution or while adsorbed to the membrane. Data shows that WKYM-NH$_2$ is released to approximately 10 μM concentration in the first 30 min of Chim2 digestion and this peptide concentration is maintained almost constant up to 480 min, while Chim2 is being hydrolyzed. The HPLC profile and MALDI-TOF mass spectrum of this experiment at t = 60 min indicates that, under this condition, the Chim2 fragments [M + H]$^{+}$ = 2332.471 Da, equivalent to KWAVKIIRKFIKG-FISGGKR, and [M + H]$^{+}$ = 2646.453 Da, KWAVKIIRK-FIKGFISGGKRWK, are significant, while other internal Chim2 trypsin peptides, which were previously detected in the same experiment using lower lipid:peptide ratios, are absent (Figs. S19, S20 and S23). This indicates that, under these conditions, Chim2 is hydrolyzed almost exclusively at the disordered Chim2b region with the concomitant release of Chim2c, the FPR2 agonist WKYM-NH$_2$, in the reaction medium. The dependence of the kinetics of Chim2 hydrolysis on the lipid:peptide molar ratios is further illustrated in the scheme presented in Figure 5I.
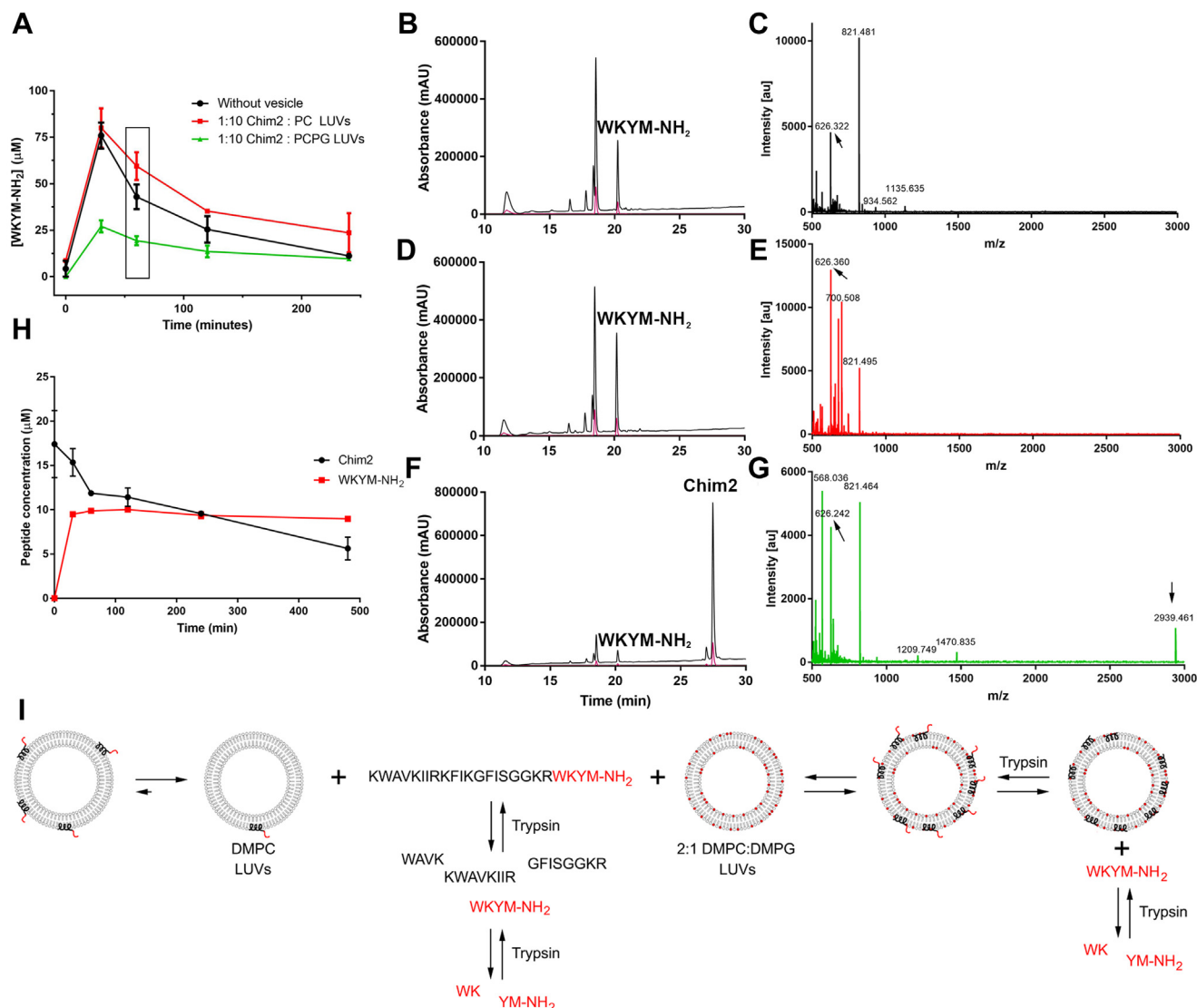
Figure 5. Kinetics of the release of the Chim2c peptide module (WKYM-NH$_2$) from Chim2 in the reaction medium analyzed by HPLC and MALDI MS. *A*, quantification of the peptide fragment WKYM-NH$_2$ as a function of the reaction time (100 μM Chim2, 1 μg/ml trypsin) without any added vesicles and with 1 mM DMPC and 1 mM 2:1 DMPC:DMPG LUVs. *Square* highlights an incubation time of 60 min. Chromatogram obtained for the injection of Chim2 samples submitted to trypsin hydrolysis for 60 min, without any added vesicle (*B*), added with 1 mM DMPC LUVs (*D*) and added with 1 mM 2:1 DMPC:DMPG LUVs (*F*). Samples were injected in an analytical C$_{18}$ column, submitted to a gradient from 0.1% TFA/water to 0.1% TFA/acetonitrile for 50 min, and sample elution was monitored in a PDA. *Black lines* correspond to sample absorption at 216 nm and *red lines* at 280 nm. WKYM-NH$_2$ was eluted at t$_r$ = 20.5 min, while Chim2 at t$_r$ = 27.5 min. MALDI-TOF/MS spectra were obtained for Chim2 hydrolyzed samples at t = 60 min in positive mode in the range m/z 500 to 3000. The mass spectrum of Chim2 trypsin hydrolyzed sample is depicted (*C*), along with samples added with 1 mM DMPC LUVs (*E*) and with 1 mM 2:1 DMPC:DMPG LUVs (*G*). *H*, the Chim2 and WKYM-NH$_2$ peptides were quantified by HPLC at t = 0, 30, 60, 120, 240, and 480 min incubation times in a second experiment, where 25 μM Chim2 was added with 1 μg/ml trypsin and 1 mM 2:1 DMPC:DMPG LUVs. *I*, illustration of the effect of vesicle adsorption on the hydrolysis of Chim2 by trypsin. When unbound, Chim2 is hydrolyzed by trypsin at several sites, including the membrane-active region Chim2a. One of the products is WKYM-NH2, which might be further hydrolyzed by trypsin itself to produce the dipeptides WK and YM-NH2. If DMPC LUVs are added, up to 1 mM concentration, the kinetics of hydrolysis is similar since the peptide does not adsorb in vesicles of this composition. If 2:1 DMPC:DMPG LUVs are added, Chim2 is adsorbed, and ideally, only the unstructured C-terminal part (-GGKRWKYM-NH2) is accessible to the enzyme. Data indicate that the higher the lipid:peptide ratio, the more dislocated the equilibrium is to the Chim2 vesicle-bound conformation and therefore, the more selective is the hydrolysis toward the C-terminal part of the molecule. LUV, large unilamellar vesicle.

Antimicrobial activity of Chim2

Given that the Chim2a module is membrane active and putatively antimicrobial since its sequence is based on the peptide Hs02, Chim2 was tested as a direct antimicrobial agent (Table 1). Chim2 presented broad antimicrobial activity, with MICs lower than 6 μM *versus* all tested bacterial strains, being therefore less potent, but comparable to Hs02 in terms of antimicrobial potency and spectra. This indicates that the peptide retains most of its antimicrobial activity, despite the introduction of Chim2b and Chim2c domains.

Production of ROS in human neutrophils

Human neutrophils from healthy donors were purified from whole blood and incubated with the peptide Chim2 and some of its tryptic fragments, more specifically, Chim2c (WKYM-NH$_2$) and the alternative Chim2 hydrolysis products,

Table 1

Minimum inhibitory and bactericidal concentrations (MIC and MBC, respectively) for Chim2 and Hs02 *versus* human pathogenic bacteria

		Microorganisms		
Peptides		*Staphylococcus aureus*	*Escherichia coli*	*Pseudomonas aeruginosa*
Chim2	MIC (μM)	4 ± 0	3.33 ± 0.94	3.33 ± 0.94
	MBC (μM)	8.00 ± 5.66	8 ± 0	6.67 ± 1.89
Hs02	MIC (μM)	2 ± 0	2 ± 0	1.67 ± 0.57
	MBC (μM)	2 ± 0	4 ± 0	ND

Abbreviation: ND, Not determined.

GGKRWKYM-NH$_2$, and GFISGGKRWKYM-NH$_2$ (Figs. S7–S12). First, the viability of neutrophils was assessed using the MTT reduction assay. For such, neutrophils were incubated with peptides at 10 μM concentration for 2 h. According to MTT assays, none of the peptides or tested conditions significantly reduced the viability of neutrophils (Fig. S24). These data were confirmed in live/dead staining assays for all molecules using LPS-primed neutrophils, except for the 10 μM Chim2, which reduced cell viability to $64 \pm 6\%$ after incubation for 30 min (Fig. S25). To verify putative cytotoxic effects of Chim2 to other cell types, we tested the cytotoxicity of this peptide in cultured fibroblasts and in fresh human erythrocytes. The peptide was indeed cytotoxic for these two cell types at a similar range of concentrations (Fig. S26). These concentrations were, however, higher than those required for the inhibition of the tested bacteria.

Quantification of ROS was performed immediately after the addition of peptide to neutrophils for 2 h (Fig. 6). The concentration of 10 μM was chosen as a compromise between the antimicrobial activity of Chim2 (inhibition and bactericidal) and the peptide cytotoxicity. In unprimed neutrophils, neither Chim2 nor Chim2c (WKYM-NH$_2$), altered the quantities of ROS in relation to untreated cells, suggesting that these peptides are unable to modulate neutrophil function without priming events (Fig. S27). However, when neutrophils were primed for 1 h with LPS, some peptides increased the production of ROS at the tested concentration in relation to control cells (Fig. 6). Chim2 and its fragment GFISGGKRW-KYM-NH$_2$ induced a fast production of ROS in LPS-primed neutrophils, a response that is consistent with FPR agonists described in the literature (36, 37). Indeed, these two peptides produced a statistically relevant increase in the production of ROS in relation to control cells (Fig. 6). Nevertheless, given that Chim2 induced the killing of neutrophils according to live/dead staining assays, a mixed mechanism of ROS production, encompassing probable FPR activation and cell death, is more likely. Peptide WKYM-NH$_2$ (Chim2c) induced no significant increase in ROS levels in neutrophils at 10 μM concentration. This indicates that Chim2c is either inactive or a weak inducer of respiratory burst in this cell type, like the annexin I peptide Ac9-25 (38). Also, while the addition of trypsin to Chim2 reversed the effects in ROS production observed for this peptide, no particular effects in ROS generation were observed. In this setting, hydrolyzed Chim2 was no longer cytotoxic toward neutrophils, but also did not induce a burst of ROS, in consonance with the low capacity displayed by
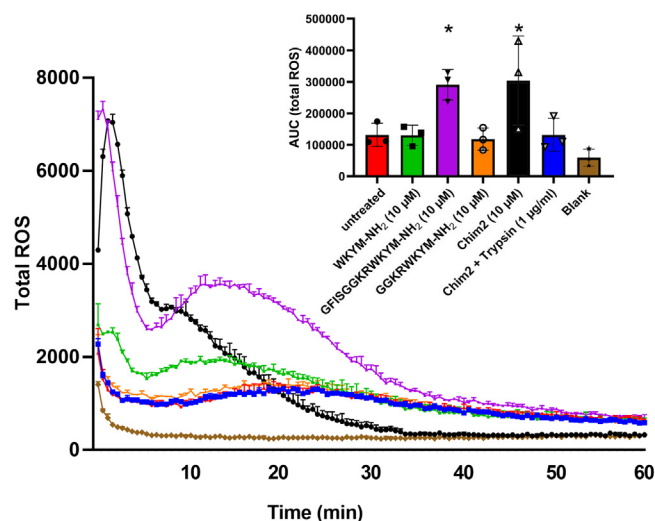
Figure 6. Total ROS production in human neutrophils primed with LPS. Human neutrophils were primed with LPS for 1 h, incubated with different peptides at 10 μM concentration, and total ROS were quantified in relation to blank and untreated cells (LPS-primed cells without peptide incubation) over 2 h. ROS areas for three independent experiments were integrated over the incubation period and are shown as an inset (mean ± SEM). *$p < 0.05$ *versus* untreated group. LPS, lipopolysaccharide; ROS, radical oxygen species.

WKYM-NH$_2$ to induce such phenomenon. We also conducted preliminary investigations using human neutrophils primed with tumor necrosis factor-α (TNF-α) (Fig. S28). The scenario is similar to that observed for LPS-primed cells, and peptides Chim2 and GFISGGKRWKYM-NH$_2$ were the most potent elicitors of ROS under these conditions.

Discussion

The present report introduces a novel strategy in the design of antimicrobial peptides, encompassing not only direct antimicrobial activity by destabilization of the prokaryote membrane but also the exploration of the local enzyme milieu for the release of immunomodulatory fragments. The strategy is similar to the recently published elastase-activated peptide-colistin conjugates (10), except that it aims not only bacterial clearance but the modulation of the immune response in the infection microenvironment. In this sense, it resembles some pepducins (39) or even gene-encoded host-defense peptides, such as the multifunctional cathelicidin peptide LL-37 (40). LL-37 is broadly antimicrobial but also binds various intracellular and transmembrane receptors, including G-protein coupled receptors, receptor tyrosine kinases, like the epidermal growth factor receptor (EGFR), and toll-like receptors (41). These interactions are thought to orchestrate the immune response against invading microorganisms (40). Such multidimensional interaction with the host immune system, although valuable, can also lead to undesired effects like autoimmune diseases through sustained feedback loops. Indeed, LL-37 is increasingly associated with psoriasis and lupus erythematosus (42). Rationally designed chimaeras, like Chim2, can thus imitate the multifunctional character of LL-37, modulating microbial growth, but activating single immunomodulatory cascades, resulting in a more controlled

interaction with host immune cells. In the present report, Chim2 was designed to activate FPR2 besides having direct antimicrobial activity. In our understanding, this is a promising bottom-up approach to the development of multifunctional peptides as customized pharmaceuticals.

An aspect that is explored in the current report is how peptide adsorption in membranes can be used to direct the enzymatic hydrolysis to certain parts of the polypeptide chain, according to their solvent exposure. This is, in our understanding, unprecedented in the literature and there are not many known natural examples of enzymatic hydrolysis of peptides while bound to membranes. One of them is the processing of the membrane-embedded AgrD molecule in the synthesis of the auto-inductor peptide in the quorum sensing of *S. aureus* (43). AgrD has a membrane-embedded part structured as an amphiphilic α-helix and a disorganized protruding tail that encompasses the *S. aureus* auto-inductor peptide, which is further processed by the membrane-bound enzymes ArgB and AgrC (44). This phenomenon resembles our results regarding the tryptic hydrolysis of the peptide Chim2 when added with model membranes. According to our data, Chim2 is unstructured in solution and attains an α-helical conformation upon adsorption to negatively charged model membranes composed of 33% DMPG. More specifically, the membrane-active part, Chim2a, transitions to an α-helix, while the Chim2b and Chim2c modules remain unstructured and highly flexible. While adsorbed to the membrane, Chim2 is hydrolyzed almost exclusively in the Chim2b and Chim2c domains, since basic residues in Chim2a are more shielded from soluble trypsin. In contrast, when titrated with zwitterionic LUVs made of DMPC that behavior is not observed. These data indicate that Chim2 might adsorb preferentially on prokaryotic membranes, which are usually negatively charged, in contrast to mammalian cells, which are formed mostly by zwitterionic phospholipids (11). Also, they suggest that the preferential hydrolysis of membrane-bound Chim2 at the Chim2b site, with the release of Chim2c, occurs only after membrane adsorption. Unbound Chim2 is thoroughly hydrolyzed, releasing multiple fragments. These data illustrate how peptides sensitive to membrane charge and curvature (45), for example, can be useful tools in the design of peptide-drug conjugates that are alternatively hydrolyzed depending on properties such as the cell type which they adsorb to. It also highlights the biotechnological potential of amphiphilic α-helices and the nuances they have in their membrane interactions, which might be useful tools in the design of peptide-drug conjugates.

It should also be emphasized that the strategy proposed herein is complex and the three modules of Chim2 must act synergistically to reach the desired effect. Also, given the interdependence of modules, *in vivo* application of this molecule may face additional challenges. At present, some improvements can be proposed. Chim2a, the membrane-active part, can possibly be made less cytotoxic and more selective toward prokaryotes by introducing point mutations or variations in size. This is currently being investigated in our group. Also, peptides, other than Hs02, might be attempted. Nevertheless, Hs02 is a suitable starting point because it is a broad and potent antimicrobial agent with anti-inflammatory activity (31). UBI29-41, although capable of discriminating bacteria from host cells, as extensively demonstrated in the literature (9), is moderately potent as an antimicrobial molecule (46) and is unlikely to adsorb to membranes to the same extent or depth as Hs02. Also, it is noteworthy that Hs02 tolerated a C-terminal expansion of 8 amino acid residues (-GGKRWKYM-NH_2) in Chim2, which modified its charge and amphiphilic balance, with little variation in its capacity to inhibit the growth of microorganisms.

The Chim2b module can also be improved, especially by altering the size or chemical nature of the spacing sequence or the enzymatic digestion site. The -KR- basic dyad in Chim2b was satisfactorily hydrolyzed by trypsin in our assays, which indicates that this site is accessible to the solubilized enzyme despite membrane adsorption of the Chim2a module. This implies that the small spacer sequence of Chim2b, -GG-, plus the unstructured Ile^{15} and Ser^{16} from Chim2a, provide enough membrane distance for the positioning of the -KR- dyad in the trypsin active site. Regarding the enzymatic specificity, relying on tryptase activity is plausible, even more at bacteria-enriched sites. Baseline trypsin-like activity in the human plasma was determined in the literature (5.48 ± 0.968 U/l) (19), and this should be augmented in case of inflammation due to activation of the complement system, among others (21). However, since trypsin-like activity is commonly encountered in human plasma, Chim2 degradation prior to reaching bacteria-infected sites should be observed. Nevertheless, the accumulation of Ubi29-41-chloramphenicol conjugates in *S. aureus* and *E. coli* infected sites in mice were shown to occur in the first 2 h of intravenous injection, despite various putative trypsin digestion sites in the Ubi29-41 molecule (9). This indicates that a fraction of the targeting peptides (Chim2 in our case) may remain integrous in this timescale, which should allow the peptide accumulation in bacteria-enriched environment. Other peptide sequences, susceptible to other enzymes from microorganisms or from the host, can, and should be explored under the same strategy, as more specificity might be gained. Leukocyte-secreted elastases and extracellular esterases are interesting alternatives and bacterial membrane-embedded or secreted enzymes should also be considered.

The Chim2c part was based in the core FPR2 agonist sequence WKYM-NH_2. This peptide was shown to increase intracellular Ca^{2+} in the rat basophilic leukemia cell line RBL-2H3 transfected with the human FPR2 complementary DNA, with an IC_{50} of 8.66 ± 4.63 nM (29). Also, it was shown to selectively activate FPR2, while other peptide from the W series also activated FPR1. In the present report, we demonstrate that BMDM, when incubated with WKYM-NH_2, accumulate lipid bodies and release IL-6 and IL-12. These are important proinflammatory cytokines with implication in the fighting off bacterial and viral infections (47, 48), signaling that this peptide has a proinflammatory overall profile. Nevertheless, this corresponds to a limited dataset regarding the immunomodulatory activity of this molecule and the panel of peptide-induced cytokines in neutrophils should be more thoroughly explored in the future.

Quantification of ROS in human neutrophils after the peptide incubation was also performed. A primary observation was that unprimed neutrophils were insensitive to the peptides or tested conditions and only primed neutrophils, with either LPS or TNF-α, responded to the treatments. This indicates that the peptides might be inactive toward this cell type outside of an inflammatory context. In LPS-primed cells, Chim2 and the fragment GFISGGKRWKYM-NH$_2$ were the most effective elicitors of ROS. The interpretation of the molecular mechanisms underlying the production of ROS in human neutrophils by Chim2 demands further experiments. Cell death, FPR activation, and suppression of LPS-induced proinflammatory response, as described for Hs02 (31), might be relevant events in the case of ROS production by Chim2. Concerning the Chim2 fragments, GFISGGKRWKYM-NH$_2$ was the most potent inducer of ROS in neutrophils in our assays. This corresponds to an alternative hydrolysis product of Chim2 that is not observed in assays using vesicles. Regarding the Chim2c fragment, WKYM-NH$_2$, no differential production of ROS in human neutrophils primed with LPS was observed. This indicates that this peptide, although capable of increasing intracellular Ca^{2+} levels through FPR2 activation in transfected cells, is a weak activator of the NADPH oxidase complex in human neutrophils. This is not unprecedented. Intracellular increase of Ca^{2+} concentration, induction of ROS formation, and neutrophil chemotaxis are some of the events that may be produced following FPR activation and they are, apparently, unrelated (37). For example, both HRYLPM-NH$_2$ and HEYLPM-NH$_2$ induced chemotaxis in human neutrophils by means of FPR2 activation but only the former induced an increase in Ca^{2+} concentrations and the generation of superoxide in the same cell type (49). Yet, such diversity in elicited intracellular cascades comes from a single amino acid substitution. Also, another possibility is that WKYM-NH$_2$ is more efficient in the activation of mice Fpr receptors than the human FPR (50), given that it induced the formation of lipid bodies in BMDM. These data suggest that WKYM-NH$_2$ demands further characterization as a FPR2 agonist in human neutrophils, which is beyond the scope of the present report, more focused in the overall design of the Chim peptides. In addition, using alternative Chim2c modules as FPR2 agonists in future generations of Chim peptides, such as WKYMVM, WKYMVm, and HFYLPM, is straightforward. Indeed, multiple peptidic and nonpeptidic FPR2 agonists have been described (51) and these may be incorporated according to their appropriateness.

In conclusion, the data described herein indicate that the Chim strategy is feasible and has potential in the generation of multifunctional peptides that are both antimicrobial and immunomodulatory. Peptides from the Chim series hold potential for *in vivo* applications, and further improvements in molecular design should come as feedback from these assays. Ideally, the peptide should be injected intravenously and a fraction of it should resist proteolysis in whole blood in a timescale that allows the peptide to accumulate in the bacteria-enriched environments, similarly to what was observed for UBI29-41-chloramphenicol conjugates (9). At present, stability in plasma (52, 53) was not addressed in the peptide design.

However, chemical modifications to increase peptide stability in blood will be attempted taking in consideration the Chim2 structural requirements: modifications in Chim2a should preserve its α-helical tendency, while those in Chim2c should preserve or enhance its capacity to bind and activate FPR2. Following accumulation in bacterial membranes, the Chim2 peptide should lower bacteria cell counts, and/or compromise their membrane integrity while activating neutrophils in the infection microenvironment. After the natural degradation of the peptide in this setting, the Chim2c portion should be produced by tryptase enzyme hydrolysis and diffuse away from the source, further activating leukocyte populations by stimulating FPR2. This is a complex script and obtaining proof-of-concept molecules that follow it is a goal that may be achieved in the future generations of optimized peptides from the Chim series.

Experimental procedures

Solid-phase synthesis, purification, and mass spectrometric analysis of peptides

Peptides were synthesized by Fmoc/tBu chemistry and peptide chain elongation was performed on a Rink amide resin, yielding C-terminal amidated molecules (54). Briefly, Rink amide resin (Novabiochem) was swollen for 20 min with dichloromethane and submitted to repeated cycles of Fmoc deprotection using 20% 4-Methylpiperidine in N,N-Dimethylformamide and peptide chain elongation using 4 equivalents of Fmoc-amino acids, N′-Diisopropylcarbodiimide, and OxymaPure, also using N,N-Dimethylformamide as solvent. After the completion of the synthesis, the N-terminal Fmoc protecting group was removed and peptide cleavage from the resin was performed using a cocktail consisting of trifluoroacetic acid:thioanisole:water:phenol:1,2-Ethanedithiol 82.5:5:5:5:2.5 (v/v) under agitation for 1.5 h. MALDI-TOF/MS analyses were performed in an UltraFlex III mass spectrometer (Bruker Daltonics) in the positive reflected mode, using α-cyano-4-hydroxicinamic acid (5 mg/ml) as ionization matrix in a proportion of 1:3, v/v in relation to the dissolved sample. Ions of interest were fragmented in the LIFT mode (MS/MS). Peptide purification was performed by RP-HPLC using a Jupiter COG 4055-P0 preparative column coupled to a Shimadzu LC-20 CE chromatographer programmed to submit samples to a linear gradient of 0.1% (v/v) TFA/acetonitrile in 0.1% (v/v) TFA/water at a flow rate of 10 ml/min. Peptide quantifications were performed by UV spectrophotometry: peptides containing Trp or Tyr residues were quantified using calculated molar absorption coefficients (55) and the remaining molecules were quantified using the UV absorbance of the peptide bond (56).

Differential scanning calorimetry and CD assays

DMPC and 2:1 DMPC:DMPG (w/w) LUVs were prepared as described in the literature (6, 7) and quantified using the ammonium ferrothiocyanate method (45). Phospholipids were weighted, dissolved in chloroform, dried in a rotary evaporator, resuspended in 20 mM sodium phosphate–NaOH, 150 mM NaCl, pH 7.4, hand-shaken until the formation of a cloudy

solution, and passed through a 100 nm polycarbonate membrane using a mini-extruder. Differential scanning calorimetry (DSC) analyses were also performed as previously described (7). Briefly, thermograms were obtained using a VP-DSC (GE Healthcare) at a temperature range from 10 to 40 °C at a scanning rate of 0.5 °C/min. Peptides were added to fresh samples of 0.5 mM LUVs at a concentration of 20 μM (0.04 mol/mol peptide/phospholipids) at room temperature, immediately followed by DSC data acquisition. Each sample was subjected to various thermal scans until there were no distinguishable changes in the thermal profile of the main phase transition ($P'_\beta \rightarrow L_\alpha$) of phospholipids between individual scans. Data was concentration normalized, baseline subtracted (linear connect), and fit to a non-two-state transition with two user-determined peaks *via* the MicroCal Origin software v7.0 (https://www.originlab.com/). Rescans for selected cases were acquired using fresh peptide and LUVs solutions to check the reproducibility of the data.

CD spectra were obtained at room temperature from 190 to 260 nm as an average of four readings using a 0.1 cm path length cell, data pitch of 0.2 nm, and a response time of 0.5 s. Data scans of the buffer solution were acquired and subtracted from each peptide scan. Peptide solutions were scanned at a concentration of 40 μM in buffer and independent samples were prepared by the addition of phospholipid LUVs of the desired composition. The spectra were converted to mean residue ellipticity and readings at 222 nm ($[\theta]_{222}$) were used to estimate helix percentages according to the literature (57).

^{1}H NMR spectroscopy and structural calculations

The lyophilized Chim2 peptide was dissolved in 600 μl of PBS buffer at pH 7.4 and water/D$_2$O (90:10, v/v) to a final peptide concentration of 2 mM in 50 mM DPC-d38. Additionally, 0.5% sodium-2,2,3,3-d4-3-trimethylsilylpropionate was added as chemical shift reference internal standard. All ^{1}H NMR experiments were performed on a Bruker Avance III HD 600 spectrometer operating at 14 T for 1 h, at 25 °C. The assignment of the peptide resonance peaks was carried out by two-dimensional experiments: TOCSY and NOESY. Two-dimensional spectra were acquired with 4096 complex points and 512 τ1 increments. The water signal was attenuated with excitation sculpting using 180 water-selective pulses. TOCSY spectra were obtained with a mixing time of 80 ms and NOESY spectra were recorded with a mixing time of 200 ms. The spectra were processed using Topspin Processor software (https://www.bruker.com/en/products-and-solutions/mr/nmr-software/topspin.html) and the contour maps were visualized using CCPNMR (version 2.4) software (https://ccpn.ac.uk/software/) (58). ^{1}H chemical shifts were assigned according to standard procedures (59). The NOE peaks were characterized based on the height of the cross-peaks. The upper bounds for the NOE constraints were calibrated according to the r-6 distance dependence of the NOE, in three classes: strong (≤1.72 Å), medium (≤3.2 Å) and weak (≤8.0 Å) (60). Structures were calculated using ARIA

(version 2.3.1) (http://aria.pasteur.fr/) (61) and CNS (version 1.2) software (http://cns-online.org/v1.3/) (62). Several cycles of ARIA were performed using standard protocols and, after each cycle, rejected restraints, violations, and assignments were analyzed. The ensemble of ten lower energy structures was chosen to represent the peptide solution 3D structure. NMR structures were deposited at the Protein Data Bank (www.rcsb.org) and were assigned with PDB ID 8EB1.

Chim2 hydrolysis assays in buffer and the presence of phospholipid LUVs

For Chim2 trypsin hydrolysis assays, DMPC and 2:1 DMPC:DMPG LUVs were made and quantified as described in Differential scanning calorimetry and CD assays. Chim2 was resuspended in 10 mM Tris-HCl, 100 mM NaCl, pH 8.0 buffer to a final concentration of 100 μM (final assay volume 100 μl) and 3 separate experiments were performed, each in duplicate: (1) Chim2 added with 6-(1-tosylamido-2-phenyl) ethyl chloromethyl ketone treated trypsin from bovine pancreas (Sigma-Aldrich) at 1 μg/ml, (2) same as experiment 1 but added with 1 mM DMPC LUVs (10:1 lipid:peptide ratio), and (3) same as experiment 1 but added with 1 mM 2:1 DMPC:DMPG LUVs LUVs (also 10:1 lipid:peptide ratio). Samples were incubated under agitation (400 rpm) at 37 °C using a Thermomixer (Eppendorf) and at time points 0, 30, 60, 120, and 240 min, 3 μl of each sample was collected for the acquisition of MALDI-TOF/MS and MS/MS spectra, which were performed as described in Solid-phase synthesis, purification, and mass spectrometric analysis of peptides. Also, 50 μl of each sample was collected, mixed with the same volume of a TFA 3% solution, and injected in a Shimadzu LC-20 CE equipped with a Vydac 254TP C$_{18}$ analytical column. Chromatographic runs were performed in gradient mode at 1 ml/min flow rate using 0.1% (v/v) TFA/water and 0.1% (v/v) TFA/acetonitrile as solvents. Peptide absorbances were measured using a diode-array detector (PDA). Previously, calibration curves were created for the peptides WKYM-NH$_2$ and Chim2, in concentrations ranging from 100 to 3.125 μM, in two-fold dilutions, in triplicates, using the same HPLC methodology, resulting in r^2 = 0.997 and 0.982 (λ = 280 nm), respectively. Calibration curves are available as supporting information Figs S21 and S22. For trypsin-digested samples, peak areas were obtained using the Post-run analysis software (https://www.shimadzu.com/an/products/software-informatics/software-option/labsolutions-cs/index.html) (Shimadzu Co) and calibration curves were used to calculate peptide concentrations. The second batch of experiments was performed, in duplicates, exactly as described, with some modifications. In these experiments, 25 μM Chim2 was used, in addition to 1 μg/ml 6-(1-tosylamido-2-phenyl) ethyl chloromethyl ketone treated trypsin, and 1 mM 2:1 DMPC:DMPG LUVs (40:1 lipid:peptide ratio), with sample incubation in the same conditions but with incubation times up to 480 min. Aliquots were also taken for MALDI-TOF/MS measurements before HPLC peak quantitation, which was performed as described. HPLC quantitative analyses were also executed as described.

Design of a membrane-active immunomodulatory peptide

IL-6 and IL-12 in murine peritoneal macrophages

BMDM from C57BL/6 were collected under the license of the animal ethics committee of the University of Brasília, nr. 17/2017. BMDM were isolated according to the literature (63) and stimulated with either Hs02 or WKYM-NH$_2$ at 10 μM and incubated for 24 h. As a positive control, cells were stimulated only with LPS (500 ng/ml) for 24 h. Supernatant IL-6 and IL-12 concentrations were detected by ELISA with a R&D Systems kit. Microtiter plates were coated overnight at room temperature with capture antibody and blocked with Reagent Diluent for 1 h. Serially diluted samples were added to the wells in triplicate and incubated overnight at 4 °C. After extensive washing, the cells were incubated with detection antibody and then Streptavidin-Horseradish Peroxidase Conjugate. After washing, the substrate solution was added and the plates were incubated for 15 min at room temperature. Plates were read after adding the stop solution at 450 nm using SpectraMax M3 spectrophotometer (Molecular Devices).

Lipid droplet biogenesis in murine peritoneal macrophages

The lipid droplets were quantitated by flow cytometry as described (31). Murine peritoneal macrophages from C57BL/6 mice were stimulated with either Hs02 or Chim2c (WKYM-NH$_2$) at 10 μM and incubated for 24 h. After, cells were dissociated with trypsin (GIBCO), washed with PBS, and incubated with the Bodipy dye (Sigma Aldrich, 50 nM) diluted in PBS for 30 min at 4 °C in the dark. Cells were washed twice with PBS, resuspended in 500 μl of PBS, and stored at 4 °C until reading by FACS Calibur using the FITC channel. FlowJo software (https://www.flowjo.com/) was used to plot data and determine the median fluorescence intensity).

Antimicrobial activity assays

The susceptibility of bacteria to the peptides described herein was tested according to the protocol M7-A10 (64) from the Clinical & Laboratory Standards Institute. Briefly, different concentrations of peptides in Mueller Hinton medium, ranging from 128 to 0.5 μM, were tested in broth dilution assays using flat bottom 96-well microplates (TPP tissue culture plates, Merck) with 5×10^5 CFU/ml of bacteria at 37 °C. The minimum inhibitory concentration was defined as the concentration at which no cells were detected in optical microscopy after 20 to 24 h incubation. For minimum microbicidal concentration determination, 10 μl of the minimum inhibitory concentration and two higher concentrations were transferred to Mueller Hinton agar plates. These plates were incubated at 37 °C for 20 to 24 h. The minimum microbicidal concentration was determined as the concentration at which no colonies were detected. All tests consisted in three biological repetitions with two technical replicates each. Tests were performed using the following strains: *S. aureus* ATCC 25923, *E. coli* ATCC 25922, and *P. aeruginosa* ATCC 27853.

MTT assays on human neutrophils

Work with human peripheral blood leukocytes complied with all relevant ethical regulations and informed consent was obtained, in accordance with the Declaration of Helsinki. The study protocol was approved by the Medical Regional Ethics Committee at the University of Edinburgh (reference number 21-EMREC-041). Human neutrophils at 10^7 cells/ml were primed with LPS (50 ng/ml) for 1 h at 37 °C (65, 66). Cells were then centrifuged and added with PBS containing Ca^{2+} and Mg^{2+} at a final concentration of 5.10^6 cells/ml. Peptides were added in different concentrations and incubated for 2 h at 37 °C. After this, cells were centrifuged and added with 350 μl MTT reagent (1:10 in PBS containing Ca^{2+} and Mg^{2+}). Cells were then distributed in flat bottomed 96-well plates at 100 μl/well. Samples were incubated for 4 h at 37 °C. Detergent was added at 100 μl/well on top of the cells and left overnight in the dark at room temperature. Readings were performed at 570 nm and 640 nm using a plate reader on the following day. MTT assays were performed in triplicates.

Neutrophil live/dead viability assays

Neutrophils were cultured in IMDM with 10% autologous serum supplemented with penicillin-streptomycin and L-glutamine (65, 67). Cells were then primed with LPS (100 ng/ml) for 1 h at 37 °C before addition of stimuli for 1 h. Chim2 was preincubated with trypsin for 30 min at 37 °C to ensure optimum peptide cleavage. Cell viability was assessed by flow cytometry (Attune NxT cytometer, Thermo Fisher Scientific) with Zombie violet live/dead stain (Biolegend, 1:400).

Measurement of NADPH oxidase activity in neutrophils

ROS production was measured indirectly using chemiluminescence production by 5×10^5 neutrophils per well at 37 °C in luminescence-grade 96-well plates (Nunc) in a Cytation plate reader (BioTek) (66). Neutrophils were first primed with either TNF-α (Sigma, 20 ng/ml) or LPS (Sigma, 50 ng/ml) for 1 h in PBS^{++} and then mixed with 150 μM luminol and 18.75 U/ml horseradish peroxidase for the analysis of total ROS production. The stimuli were added to the cells and the luminescence was recorded immediately for a total of 2 h. Data output was in light units per second and experiments were performed in technical duplicates for LPS-primed neutrophils (n = 3 healthy donors) as well as for TNF-α primed cells (n = 1 donor).

Cell viability assays and hemolysis test

Human fibroblast cell (Detroit 551) was obtained from Rio de Janeiro Cell Bank (BCRJ). Cells were cultured in DMEM (Gibco BRL) supplemented with 10% heat inactivated fetal bovine serum (Gibco) and 1% antibiotic solution (10,000 U/ml penicillin and 10 mg/ml streptomycin, Sigma-Aldrich) at 37 °C and 5% CO$_2$ in a humidified atmosphere. The cells were seeded into 96-well culture plate at a density of 3×10^3 and maintained for 24 h. Then, the cells were treated with peptide diluted in DMEM medium at a concentration range from 128 to 4 μM, in triplicates. DMEM medium and 20% DMSO (dimethylsulfoxide) were used as controls. The plates were incubated for 24 and 48 h, and the cell viability was evaluated

by MTT (3-[4,5-dimethylthiazol-2-yl]-2,5-diphenyltetrazolium bromide, Sigma-Aldrich) dye reduction method. After exposure time, the medium was removed and 100 µl of MTT solution diluted in DMEM (0.75 mg/ml) was added in each well and incubated for 2 h at 37 °C. Dimethylsulfoxide (100 µl) was then added to dissolve the formazan salts produced by living cells. The absorbance was measured at 595 nm using a SpectraMax Plus 384 microplate reader (Molecular Devices). For hemolysis tests, the peripheral blood was obtained with EDTA (1.8 mg/ml) from one volunteer human donor. The blood was centrifuged for 10 min at 1500 rpm and the erythrocytes were washed three times with 1× PBS at 37 °C. The erythrocyte suspension was adjusted to reach 5% of cells in 1× PBS. Then, 80 µl of this solution was added to 20 µl of Chim2 diluted in 1× PBS, with concentrations ranging from 128 to 1 µM. The samples were incubated for 1 h at 37 °C, and after that the reaction was interrupted by adding 100 µl of 1× PBS. Samples were centrifuged at 4700 rpm for 5 min and the supernatant was measured at 550 nm using a SpectraMax Plus 384 microplate reader (Molecular Devices). The negative (absence of hemolysis) and positive (100% hemolysis) controls were set with 1× PBS and Triton-X 100, respectively.

Statistical analysis

Data analyses were performed using GraphPad Prism version 7.0 (GraphPad Softwares) (https://www.graphpad.com/features). One-way ANOVA was performed with Dunnett's post hoc tests to verify differences between groups in assays involving neutrophils. Alternatively, for cell viability assays in fibroblasts and hemolysis assays, ANOVA was followed by Bonferroni's multiple comparison analyses to verify statistical differences between groups. Two-way ANOVA followed by Bonferroni's multiple comparison analyses were employed to compare means between the exposure times 24 and 48 h. Differences between means were considered statistically significant at $p < 0.05$. The data were expressed as mean ± SEM of the triplicate from two independent experiments.

Data availability

Data is available upon request. Please contact Guilherme D. Brand (gdbrand@unb.br).

References

1. Last, N. B., Schlamadinger, D. E., and Miranker, A. D. (2013) A common landscape for membrane-active peptides. *Protein Sci.* 22, 870–882
2. Avci, F. G., Akbulut, B. S., and Ozkirimli, E. (2018) Membrane active peptides and their biophysical characterization. *Biomolecules* 8, 77
3. Neundorf, I. (2019) Antimicrobial and cell-penetrating peptides: how to understand two distinct functions despite similar physicochemical properties. In: Matsuzaki, K., ed. *Antimicrobial Peptides: Basics for Clinical Application*, Springer Singapore, Singapore: 93–109
4. Vigant, F., Santos, N. C., and Lee, B. (2015) Broad-spectrum antivirals against viral fusion. *Nat. Rev. Microbiol.* 13, 426–437
5. Hebda, J. A., and Miranker, A. D. (2009) The interplay of catalysis and toxicity by amyloid Intermediates on lipid bilayers: insights from type II diabetes. *Annu. Rev. Biophys.* 38, 125–152
6. Reinhardt, A., and Neundorf, I. (2016) Design and application of antimicrobial peptide conjugates. *Int. J. Mol. Sci.* 17, 701
7. Albada, B., and Metzler-Nolte, N. (2017) Highly potent antibacterial organometallic peptide conjugates. *Acc. Chem. Res.* 50, 2510–2518
8. Akhtar, M. S., Imran, M. B., Nadeem, M. A., and Shahid, A. (2012) Antimicrobial peptides as infection imaging agents: better than radio-labeled antibiotics. *Int. J. Pept.* 2012, 1–19
9. Chen, H., Liu, C., Chen, D., Madrid, K., Peng, S., Dong, X., *et al.* (2015) Bacteria-targeting conjugates based on antimicrobial peptide for bacteria diagnosis and therapy. *Mol. Pharm.* 12, 2505–2516
10. Tegge, W., Guerra, G., Höltke, A., Schiller, L., Beutling, U., Harmrolfs, K., *et al.* (2021) Selective bacterial targeting and infection-triggered release of antibiotic colistin conjugates. *Angew. Chem. Int. Ed. Engl.* 60, 17989–17997
11. Yeaman, M. R., and Yount, N. Y. (2003) Mechanisms of antimicrobial peptide action and resistance. *Pharmacol. Rev.* 55, 27–55
12. Yount, N. Y., Weaver, D. C., Lee, E. Y., Lee, M. W., Wang, H., Chan, L. C., *et al.* (2019) Unifying structural signature of eukaryotic α-helical host defense peptides. *Proc. Natl. Acad. Sci. U. S. A.* 116, 6944–6953
13. Ebenhan, T., Gheysens, O., Kruger, H. G., Zeevaart, J. R., and Sathekge, M. M. (2014) Antimicrobial peptides: their role as infection-selective tracers for molecular imaging. *Biomed. Res. Int.* 2014, 867381
14. Savini, F., Luca, V., Bocedi, A., Massoud, R., Park, Y., Mangoni, M. L., *et al.* (2017) Cell-density dependence of host-defense peptide activity and selectivity in the presence of host cells. *ACS Chem. Biol.* 12, 52–56

15. Rosa, L. M., Filippo, S., Sara, B., Bruno, C., Henrik, F., Luisa, M. M., *et al.* (2021) Inoculum effect of antimicrobial peptides. *Proc. Natl. Acad. Sci. U. S. A.* **118**, e2014364118

16. Akhtar, M. S., Qaisar, A., Irfanullah, J., Iqbal, J., Khan, B., Jehangir, M., *et al.* (2005) Antimicrobial peptide 99mTc-ubiquicidin 29-41 as human infection-imaging agent: clinical trial. *J. Nucl. Med.* **46**, 567–573

17. Starr, C. G., and Wimley, W. C. (2017) Antimicrobial peptides are degraded by the cytosolic proteases of human erythrocytes. *Biochim. Biophys. Acta Biomembr.* **1859**, 2319–2326

18. Poreba, M. (2020) Protease-activated prodrugs: strategies, challenges, and future directions. *FEBS J.* **287**, 1936–1969

19. Hernandez, C. A., Nicolas, J. C., Bioch, D., Fernandez, J., and Pizarro, P. (2005) Determination of plasma trypsin-like activity in healthy subjects, patients with mild to moderate alcoholic chronic pancreatitis, and patients with nonjaundice pancreatic cancer. *Dig. Dis. Sci.* **50**, 2165–2169

20. Ramachandran, R., Altier, C., Oikonomopoulou, K., and Hollenberg, M. D. (2016) Proteinases, their extracellular targets, and inflammatory signaling. *Pharmacol. Rev.* **68**, 1110

21. Nickel, K. F., and Renné, T. (2012) Crosstalk of the plasma contact system with bacteria. *Thromb. Res.* **130**, S78–S83

22. Weidmann, H., Heikaus, L., Long, A. T., Naudin, C., Schlüter, H., and Renné, T. (2017) The plasma contact system, a protease cascade at the nexus of inflammation, coagulation and immunity. *Biochim. Biophys. Acta Mol. Cell Res.* **1864**, 2118–2127

23. Weiß, E., and Kretschmer, D. (2018) Formyl-peptide receptors in infection, inflammation, and cancer. *Trends Immunol.* **39**, 815–829

24. Li, L., Chen, K., Xiang, Y., Yoshimura, T., Su, S., Zhu, J., *et al.* (2016) New development in studies of formyl-peptide receptors: critical roles in host defense. *J. Leukoc. Biol.* **99**, 425–435

25. Weiss, E., Hanzelmann, D., Fehlhaber, B., Klos, A., von Loewenich, F. D., Liese, J., *et al.* (2018) Formyl-peptide receptor 2 governs leukocyte influx in local staphylococcus aureus infections. *FASEB J.* **32**, 26–36

26. Kim, S. D., Kim, Y.-K., Lee, H. Y., Kim, Y.-S., Jeon, S. G., Baek, S.-H., *et al.* (2010) The agonists of formyl peptide receptors prevent development of severe sepsis after microbial infection. *J. Immunol.* **185**, 4302–4310

27. Cattaneo, F., Parisi, M., and Ammendola, R. (2013) Distinct signaling cascades elicited by different formyl peptide receptor 2 (FPR2) agonists. *Int. J. Mol. Sci.* **14**, 7193–7230

28. Kim, S. D., Kim, J. M., Jo, S. H., Lee, H. Y., Lee, S. Y., Shim, J. W., *et al.* (2009) Functional expression of formyl peptide receptor family in human NK cells. *J. Immunol.* **183**, 5511

29. Wan, H.-X., Zhou, C., Zhang, Y., Sun, M., Wang, X., Yu, H., *et al.* (2007) Discovery of Trp-Nle-Tyr-Met as a novel agonist for human formyl peptide receptor-like 1. *Biochem. Pharmacol.* **74**, 317–326

30. Brand, G. D., Magalhães, M. T. Q., Tinoco, M. L. P., Aragão, F. J. L., Nicoli, J., Kelly, S. M., *et al.* (2012) Probing protein sequences as sources for encrypted antimicrobial peptides. *PLoS One* **7**, e45848

31. Brand, G. D., Moraes, J. de, Ramada, M. H. S., Manickchand, J. R., Correa, R., Ribeiro, D. J. S., *et al.* (2019) Intragenic antimicrobial peptides (IAPs) from human proteins with potent antimicrobial and anti-inflammatory activity. *PLoS One* **14**, e0220656

32. Mariano, G. H., Gomes de Sá, L. G., Carmo da Silva, E. M., Santos, M. A., Cardozo Fh, J. L., Lira, B. O. V., *et al.* (2021) Characterization of novel human intragenic antimicrobial peptides, incorporation and release studies from ureasil-polyether hybrid matrix. *Mater. Sci. Eng. C Mater. Biol. Appl.* **119**, 111581

33. D, M. J., Daren, E., Kevin, S., Steve, R., F, K. J., and George, G. (2004) Substrate specificity of the Escherichia coli outer membrane protease OmpT. *J. Bacteriol.* **186**, 5919–5925

34. Epand, R. M., and Sturtevant, J. M. (1981) A calorimetric study of peptide-phospholipid interactions: the glucagon-dimyristoylphosphatidylcholine complex. *Biochemistry* **20**, 4603–4606

35. Brand, G. D., Ramada, M. H. S., Genaro-Mattos, T. C., and Bloch, C. (2018) Towards an experimental classification system for membrane active peptides. *Sci. Rep.* **8**, 1194

36. Christophe, T., Karlsson, A., Dugave, C., Rabiet, M.-J., Boulay, F., and Dahlgren, C. (2001) The synthetic peptide Trp-Lys-Tyr-Met-Val-Met-NH_2 specifically activates neutrophils through FPRL1/lipoxin A_4 receptors and is an agonist for the orphan monocyte-expressed chemo-attractant receptor FPRL2 *. *J. Biol. Chem.* **276**, 21585–21593

37. Bae, Y.-S., Park, J. C., He, R., Ye, R. D., Kwak, J.-Y., Suh, P.-G., *et al.* (2003) Differential signaling of formyl peptide receptor-like 1 by Trp-Lys-Tyr-Met-Val-Met-$CONH_2$ or lipoxin A4 in human neutrophils. *Mol. Pharmacol.* **64**, 721

38. Walther, A., Riehemann, K., and Gerke, V. (2000) A novel ligand of the formyl peptide receptor: annexin I regulates neutrophil extravasation by interacting with the FPR. *Mol. Cell* **5**, 831–840

39. Malene, W., Michael, G., I, O. T., Bodil, J., Francois, B., Johan, B., *et al.* (2014) Antibacterial activity of pepducins, allosterical modulators of formyl peptide receptor signaling. *Antimicrob. Agents Chemother.* **58**, 2985–2988

40. Vandamme, D., Landuyt, B., Luyten, W., and Schoofs, L. (2012) A comprehensive summary of LL-37, the factotum human cathelicidin peptide. *Cell Immunol.* **280**, 22–35

41. Verjans, E.-T., Zels, S., Luyten, W., Landuyt, B., and Schoofs, L. (2016) Molecular mechanisms of LL-37-induced receptor activation: an overview. *Peptides* **85**, 16–26

42. Kahlenberg, J. M., and Kaplan, M. J. (2013) Little peptide, big effects: the role of LL-37 in inflammation and autoimmune disease. *J. Immunol.* **191**, 4895–4901

43. Zhang, L., Lin, J., and Ji, G. (2004) Membrane anchoring of the AgrD N-terminal amphipathic region is required for its processing to produce a quorum-sensing pheromone in staphylococcus aureus*. *J. Biol. Chem.* **279**, 19448–19456

44. Wang, B., and Muir, T. W. (2016) Regulation of virulence in staphylococcus aureus: molecular mechanisms and remaining puzzles. *Cell Chem. Biol.* **23**, 214–224

45. Koller, D., and Lohner, K. (2014) The role of spontaneous lipid curvature in the interaction of interfacially active peptides with membranes. *Biochim. Biophys. Acta* **1838**, 2250–2259

46. Brouwer, C. P. J. M., Bogaards, S. J. P., Wulferink, M., Velders, M. P., and Welling, M. M. (2006) Synthetic peptides derived from human antimicrobial peptide ubiquicidin accumulate at sites of infections and eradicate (multi-drug resistant) staphylococcus aureus in mice. *Peptides* **27**, 2585–2591

47. Hamza, T., Barnett, J. B., and Li, B. (2010) Interleukin 12 a key immuno-regulatory cytokine in infection applications. *Int. J. Mol. Sci.* **11**, 789–806

48. Petri, W. A., Nerida, C., Mark, K., Shisan, B., W, B. K., J, H. A., *et al.* (2001) Effects of exogenous interleukin-6 during Pseudomonas aeruginosa corneal infection. *Infect. Immun.* **69**, 4116–4119

49. Bae, Y.-S., Yi, H. J., Lee, H.-Y., Jo, E. J., Kim, J. I., Lee, T. G., *et al.* (2003) Differential activation of formyl peptide receptor-like 1 by peptide ligands. *J. Immunol.* **171**, 6807

50. Winther, M., Dahlgren, C., and Forsman, H. (2018) Formyl peptide receptors in mice and men: similarities and differences in recognition of conventional ligands and modulating lipopeptides. *Basic Clin. Pharmacol. Toxicol.* **122**, 191–198

51. Maciuszek, M., Cacace, A., Brennan, E., Godson, C., and Chapman, T. M. (2021) Recent advances in the design and development of formyl peptide receptor 2 (FPR2/ALX) agonists as pro-resolving agents with diverse therapeutic potential. *Eur. J. Med. Chem.* **213**, 113167

52. Böttger, R., Hoffmann, R., and Knappe, D. (2017) Differential stability of therapeutic peptides with different proteolytic cleavage sites in blood, plasma and serum. *PLoS One* **12**, e0178943

53. Werner, H. M., Cabalteja, C. C., and Horne, W. S. (2016) Peptide backbone composition and protease susceptibility: impact of modification type, position, and tandem substitution. *Chem. Bio. Chem.* **17**, 712–718

54. Chan, W., and White, P. (2000) *Fmoc Solid Phase Peptide Synthesis: A Practical Approach*, Oxford University Press, Oxford

55. Kirschenbaum, D. M. (1975) Molar absorptivity and A-1% 1cm values for proteins at selected wavelengths of the ultraviolet and visible regions. X. *Anal. Biochem.* **64**, 186–213

56. Wadell, W. J. (1956) A simple UV spectrophotometric method for the determination of protein. *J. Lab. Clin. Med.* **48**, 311–314

57. Chen, Y. H., Yang, J. T., and Chau, K. H. (1974) Determination of the helix and beta form of proteins in aqueous solution by circular dichroism. *Biochemistry* **13**, 3350–3359

58. Vranken, W. F., Boucher, W., Stevens, T. J., Fogh, R. H., Pajon, A., Llinas, M., *et al.* (2005) The CCPN data model for NMR spectroscopy: development of a software pipeline. *Proteins* **59**, 687–696

59. Wüthrich, K. (1986) *NMR of Proteins and Nucleic Acids*. Wiley-Interscience, New Jersey

60. Skinner, S. P., Goult, B. T., Fogh, R. H., Boucher, W., Stevens, T. J., Laue, E. D., *et al.* (2015) Structure calculation, refinement and validation using *CcpNmr Analysis. Acta Crystallogr. D Biol. Crystallogr.* **71**, 154–161

61. Rieping, W., Habeck, M., Bardiaux, B., Bernard, A., Malliavin, T. E., and Nilges, M. (2007) ARIA2: automated NOE assignment and data integration in NMR structure calculation. *Bioinformatics* **23**, 381–382

62. Brunger, A. T. (2007) Version 1.2 of the crystallography and NMR system. *Nat. Protoc.* **2**, 2728–2733

63. Marim, F. M., Silveira, T. N., Lima, D. S., Jr., and Zamboni, D. S. (2010) A method for generation of bone marrow-derived macrophages from cryopreserved mouse bone marrow cells. *PLoS One* **5**, e15263

64. CLSI (2015). In *M07-A10: Methods for Dilution Antimicrobial Susceptibility Tests for Bacteria That Grow Aerobically; Approved Standard— Tenth Edition* (vol. 35,. Clinical and Laboratory Standards Institute, Wayne, PA: 1–87

65. Barth, N. D., Subiros-Funosas, R., Mendive-Tapia, L., Duffin, R., Shields, M. A., Cartwright, J. A., *et al.* (2020) A fluorogenic cyclic peptide for imaging and quantification of drug-induced apoptosis. *Nat. Commun.* **11**, 4027

66. Karmakar, U., Chu, J. Y., Sundaram, K., Astier, A. L., Garside, H., Hansen, C. G., *et al.* (2021) Immune complex-induced apoptosis and concurrent immune complex clearance are anti-inflammatory neutrophil functions. *Cell Death Dis.* **12**, 296

67. Ren, C., Yuan, Q., Jian, X., Randazzo, P. A., Tang, W., and Wu, D. (2020) Small GTPase ARF6 is a coincidence-detection code for RPH3A polarization in neutrophil polarization. *J. Immunol.* **204**, 1012–1021